https://doi.org/10.1016/j.trgeo.2020.100345

Compression and wetting induced volumetric behavior of loess: macro- and micro-investigations

Authors: Q. Y. Mu, C. Zhou* and C. W. W. Ng

*Corresponding author

Manuscript Type: Technical paper

Information of the authors

Q. Y. Mu

Assistant Professor, Department of Civil Engineering, Xi'an Jiaotong University, Xi'an, P. R. China;

E-mail: qingyimu@mail.xjtu.edu.cn

C. Zhou

Assistant Professor, Department of Civil and Environmental Engineering, the Hong Kong Polytechnic University, Hong Kong SAR

E-mail: c.zhou@polyu.edu.hk

C. W. W. Ng

CLP Holdings Professor of Sustainability, Department of Civil and Environmental Engineering, the Hong Kong University of Science and Technology, Hong Kong SAR

E-mail: cecwwng@ust.hk

Abstract

Volumetric behavior of loess induced by isotropic compression and wetting was investigated through stress- and suction-controlled triaxial tests. To assist in the interpretation of test results, X-ray diffraction (XRD), Scanning Electron Microscope (SEM) and Mercury Intrusion Porosimeter (MIP) tests were carried out to determine the mineral composition and the microstructure of the tested loess. Results of compression tests showed that yield stresses of intact loess were larger than that of the compacted loess because of stabilization effects contributed by clay particles and calcite in intact loess, as evidenced by SEM and XRD results. On the other hand, constant water content was observed for intact loess during compression at suctions 50 kPa and 100 kPa, while the water content of compacted loess increased by 4.4% and 7.4% respectively. MIP tests revealed that compression of the intact loess mainly occurred in the extra-large pores, but with minuscule effects on the pores governing water distribution at suctions 50 kPa and 100 kPa. For compacted loess, a number of inter-aggregate pores were compressed below the pore diameters responsible for water flowing in the pores at the applied suctions. In addition, intact loess showed wetting induced swelling at an isotropic stress of 50 kPa, while collapse was observed for compacted loess with the same stress path.

Key words: loess; volumetric behavior; microstructure; mineral composition

1. Introduction

Loess deposits are widely distributed in China, Iran and Europe (Muñoz-Castelblanco et al., 2011; Garakani et al., 2015; Jiang et al., 2016). Among these regions, the loess plateau in northwest China has the most extensive loess deposits consisting of layers with great thickness (Ma et al., 2017). According to previous studies, loess is a well-known collapse soil because of the metastable structure (Liu et al., 2015; Ng et al., 2016a). During mechanical loading or wetting, significant collapse can be induced which leads to settlement or failure of subgrades (Jiang et al., 2016; Garakani et al., 2018; Ji et al., 2018). Furthermore, collapse behavior of unsaturated soil induced by mechanical loading and wetting are closely interrelated according to the elasto-plastic theory (Alonso et al., 1990). So far, researchers have carried out extensive studies on the collapse behavior of loess (Wang et al., 2014; Jiang et al., 2012; Liu et al., 2015; Garakani et al., 2015; Haeri et al., 2016; Ng et al., 2016b; Ji et al, 2019). However, investigations on the compression and wetting induced volumetric behavior of loess from the viewpoints of macro- and micro-structures are still incomplete.

To note, most of the previous studies related to the compression and wetting induced volumetric behavior of loess focused either on intact or compacted samples. Muñoz-Castelblanco et al. (2011) studied the compression and wetting induced collapse behavior of intact loess by carrying out oedometric compression tests. Their results showed that both compression and wetting induced plastic strains changed the shape of loading collapse (LC) curve. Jiang et al. (2012) studied the wetting

induced collapse behavior of artificial loess through single- and double-oedometer tests. The results showed that the tested loess displayed a maximum wetting induced collapse when the stress was equal to the yield stress. In addition, the wetting-induced collapse behavior was independent of the sequence of wetting and mechanical loadings. Liu et al. (2015) analyzed the collapse behavior of intact loess with respect to its microstructure. A conceptual microstructure model that considered clay connections and cementation minerals was proposed to interpret the wetting induced collapse. On the other hand, Garakani et al. (2015) characterized the hydro-mechanical behavior of intact loess from northeast Iran. It was found that the magnitude and extent of collapse are different depending on the applied stress and the hydro-mechanical loading path. For comparison studies of intact and compacted loess, Ng et al. (2018) carried out temperature-controlled triaxial tests to investigate the collapse behavior of loess. They concluded that wetting induced collapse of intact and compacted loess showed different trends when the confining stress increases from 50 kPa to 110 kPa. However, microstructure analysis, which could have thrown a clearer picture of the underlying mechanisms of the collapse behavior of loess was not included.

In the present work, the volumetric behavior of intact and compacted loess was explored by carrying out a series of isotropic compression tests and a series of wetting tests using an unsaturated triaxial apparatus. The behavior of compacted loess can provide a base for better understanding of structural effects on the volume change behavior of loess. X-ray diffraction (XRD), Scanning Electron Microscope

(SEM) and Mercury Intrusion Porosimeter (MIP) tests were carried out to get an insight of the underlying mechanisms of the volumetric behavior of the loess. The macro- and micro- investigations together with the composition analysis of this study are expected to provide helpful guidance on evaluating the collapsibility of loess.

2. Test material and sample preparation methods

2.1. Test material

High quality loess block samples (25cm×25cm×25cm) were collected from an excavated pit in Xi'an, Shaanxi province of China. The in-situ gravimetric water content and dry density were 6.31% and 1.30 g/cm^3, respectively. The liquid limit and plastic limit were 36% and 19%, respectively. According to ASTM D 2487 (ASTM, 2006), the loess was classified as clay of low plasticity. More details of the physical properties of the tested loess can be found in Ng et al. (2016a).

XRD test was carried out to identify the mineral compositions of the tested loess. Figure 1 shows the XRD pattern of the intact loess. The peaks in the range of 5^o-20^o and 20^o-40^o represent clay and non-clay minerals, respectively. It can be seen that the peaks in the range 20^o-40^o are larger than those in the range 5^o-20^o, indicating that non-clay minerals dominated the composition of the tested loess. The non-clay minerals, such as quartz (Q), albite (A) and calcite (C) were identified. It should be noted that the calcite is a cementation material which was probably acquired from the initial wind deposition or reprecipitation (Liu et al., 2015;

Behnood, 2018). On the other hand, the clay minerals of the tested loess included nimite (N) and muscovite (M).

2.2. Sample preparation methods

To prepare intact loess samples, small blocks of size 50 mm × 50 mm × 100 mm were cut from the bulk material. The small block was next trimmed on a lathe to a cylinder of 76 mm in height and 38 mm in diameter. The detailed soil states of each sample are given in Table 1.

To prepare compacted samples, the loess was first air-dried, then crushed and passed through a 1.18 mm British standard sieve. The loess powder was mixed with de-aired water so that the gravimetric water content was equal to that of intact samples. The mixed soil was passed through the 1.18 mm British standard sieve again to reduce the clog size (Zhan et al., 2014). The compacted samples were then obtained by static compaction of the mixed loess powder in a split mould, targeting the average dry density of the intact samples.

3. Test apparatus

An unsaturated Global Digital Systems (GDS) triaxial cell was utilized for isotropic compression and wetting tests. The suction of soil sample (u_a-u_w) was controlled via axis translation technique, by controlling the air pressure (u_a) and pore water pressure (u_w). The volumetric strain of the unsaturated soil sample was measured by using a double cell system. This double cell system uses an accurate differential pressure transducer to record any changes in the differential pressure which occur due to changes in water level within the inner cell caused by volume

change of the soil sample (Ng et al., 2018). The accuracy of the volume change measuring system was 0.04% for the tested samples.

To investigate the microstructure of the tested samples, SEM and MIP tests were carried out. For the SEM tests, the JSM-7100F (Japan Electron Optics 192 Laboratory, JEOL) was used. For the MIP tests, Auto Pore IV 9500 V1.04 instrument with both low- and high-pressure ports was used. Furthermore, since both SEM and MIP tests accept dry samples, freeze-drying method similar to that of Delage et al. (1996) was done to dehydrate the soil samples. Samples were first dipped in liquid nitrogen, followed by placing them in an Edwards Super Modulyo apparatus to remove all frozen water. The prepared samples for SEM and MIP tests have approximate dimensions of 5 mm×5 mm×5 mm.

4. Test program and test procedure

4.1. Test program

The current study included two series of tests. In the first series, the isotropic compression behavior of intact and compacted loess was studied at constant suctions. The suctions applied were zero kPa, 50 kPa and 100 kPa. The second test series was designed to study the wetting induced volume change behavior of the loess samples. The volume changes of intact and compacted loess were measured by carrying out wetting tests at constant isotropic stresses of zero kPa, 50 kPa and 200 kPa. The soil states for each test are given in Table 1. To further understand the underlying mechanisms of compression and wetting-induced volume change behavior,

microstructural study of the loess was necessary. Such analysis was done through SEM and MIP tests in its initial state and after isotropic compression.

4.2. Test procedure

Figure 2a shows the stress paths of each test in the isotropic compression study. Each soil sample (i.e., IS100, CS100, IS50, CS50, IS0 and CS0) was first wetted by decreasing the suction from the initial value (about 1250 kPa) to 100 kPa, 50 kPa and zero kPa (A0→B0, A0→C0 and A0→D0). The soil samples were then subjected to suction equalization. The suction equalization was considered to be finished when the water content change was smaller than 0.04%/day (Sivakumar, 1993). After suction equalization, the soil samples were compressed by increasing the net mean stress from 0 to 300 kPa (i.e. B0→B1, C0→C1 and D0→D1). Figure 2b shows the hydro-mechanical paths of each test in the wetting tests. Each soil sample (i.e. IP200, CP200, IP50, CP50, IP0 and CP0) was first wetted by decreasing the suction from the initial value (about 1250 kPa) to 200 kPa (A0→B0). Thereafter, the soil samples were compressed by increasing the net mean stress from zero to 50 kPa and 200 kPa under constant suction conditions (B0→B1 and B0→B2). Then, the suction of each soil sample was decreased from 200 to zero kPa under constant isotropic stresses (B0→C0, B1→C1 and B2→C2).

5. Experimental results

5.1. Compression induced volume change of intact and compacted loess

5.1.1. Intact loess

Figure 3a shows isotropic compression curves of intact loess at suctions of zero kPa, 50 kPa and 100 kPa. For the intact loess at zero kPa suction, the relationship between void ratio and net mean stress was highly non-linear. The pseudo-elastic and plastic sections were clearly identifiable from the compression curve. The yield stress, defined as intersection of these two lines, was 28.2 kPa. On the other hand, the value of compressibility index (λ), which is the slope of the linear segment of the plastic section, was 0.175. For the intact samples at suctions of 50 kPa and 100 kPa, the variations of void ratio with the net mean stress showed similar patterns to that of the intact loess at suction of zero kPa. The yield stresses of the intact samples at suctions of 50 kPa and 100 kPa were 112.4 kPa and 178.3 kPa, respectively. As expected, the yield stress of the intact loess decreased with a decrease in the suction. This was mainly because of the wetting induced softening of the soil skeleton. First, a decrease in the suction reduced the amount of meniscus water, which provided stabilizing effects on the soil skeleton (Wheeler et al. 2003; Mu et al., 2018). On the other hand, our tested loess belongs to the category of cemented unsaturated soils because of clay connections (see detailed explanations in section 6) and calcite cementation (see the XRD result in Figure 1). The stabilizing effects contributed by the clay connections can be partially erased with wetting (Muñoz-Castelblanco et al., 2012; Mu et al., 2020). On the other hand, the λ values of the intact loess at suctions of 50 kPa and 100 kPa were 0.166 and 0.168, respectively, and no clear trend between the λ and soil suction was observed within the suction range studied.

Figure 3b shows the changes in gravimetric water content of intact loess during isotropic compression at suctions of zero, 50 kPa and 100 kPa. At suction zero kPa, the gravimetric water content of the intact loess decreased significantly with an increase in the net mean stress. It was consistent with the deformation behavior shown in Figure 3a. Water was drained out of pores in the saturated sample with soil compression. On the other hand, at suctions 50 kPa and 100 kPa, the gravimetric water content of the intact loess remained almost unchanged with increase in the net mean stress from zero to 300 kPa. This constant water content seemed contradictory to the deformation behavior of the intact loess shown in Figure 3a. The reason for such contradiction was that the compression of intact loess occurred due to breaking of extra-large pores with little effects on the pores that govern water content change at suctions of 50 and 100 kPa. This explanation was further supported by the MIP measurements as described in section 6. Similar test results were obtained by Muñoz-Castelblanco et al. (2011) who observed constant suctions during oedometric compression of unsaturated intact loess under constant water content conditions.

5.1.2. Compacted loess

Figure 4a shows isotropic compression curves of compacted loess at suctions zero kPa, 50 kPa and 100 kPa. All the three curves showed clear pseudo-elastic and plastic segments, which were similar to that of the intact loess shown in Figure 3a. The yield stresses of the compacted loess at suctions zero kPa, 50 kPa and 100 kPa were 16.2 kPa, 63.4 kPa and 84.7 kPa, respectively. Similar to the intact loess, the yield stress of the compacted loess decreased with decreasing the suction. As the

clay connections and calcite cementation were destroyed during sample preparation, wetting induced softening of the soil skeleton of compacted loess might be solely attributed to the reduction in amount of meniscus water. Furthermore, the yield stresses of intact loess at suctions zero kPa, 50 kPa and 100 kPa were 42.3%, 43.6% and 52.5% larger than that of the compacted loess, respectively. The stiffer soil skeleton of the intact loess at suctions 50 kPa and 100 kPa was due to the stabilizing effects contributed by clay connections and calcite cementation. At suction of zero kPa, the larger yield stress of the intact loess could be mainly attributed to the calcite cementation as the clay connections was partially destroyed in the saturated state (Muñoz-Castelblanco et al., 2012; Ng et al., 2019).

Figure 4b shows gravimetric water content changes for the compacted loess at suctions zero kPa, 50 kPa and 100 kPa. At suction zero kPa, the gravimetric water content of the compacted loess decreased significantly with increasing net mean stress. It was consistent with the contractive behavior of the compacted soil (see Figure 4a) as explained in section 5.1.1. More importantly, the gravimetric water content of the compacted loess increased with an increase in the net mean stress at suctions 50 kPa and 100 kPa. It was different from the intact loess which showed a constant gravimetric water content during its isotropic compression (see Figure 3b). This was mainly because during isotropic compression, the size of a number of inter-aggregated pores in the compacted loess decreased and went below a critical dimension. Such decrease led the water to flow in the soil samples at the applied suctions 50 kPa and 100 kPa. A more detailed explanation has been provided in

section 6 with respect to the microstructure changes of the tested loess during compression.

5.2. Wetting-induced volume change of intact and compacted loess

Figure 5 shows the wetting induced volume change behavior of both intact and compacted loess under constant isotropic stress conditions. For the intact loess, swellings were observed at isotropic stresses of zero kPa and 50 kPa. At the isotropic stress of 200 kPa, the intact stress first showed swelling with decreasing suctions from 200 kPa to about 100 kPa, and finally a collapse strain of 13.7% was observed at suctions further decreasing from 100 kPa to zero kPa. For the compacted loess, a similar wetting induced swelling behavior to that of the intact loess was observed at zero kPa isotropic stress. Furthermore, at isotropic stress of 50 kPa, the compacted loess exhibited a wetting induced collapse strain of 7.9%. It became apparent that the wetting induced volume change behaviors of intact and compacted loess was just opposite at 50 kPa isotropic stress. In addition, at isotropic stress of 200 kPa, the compacted loess showed a collapse strain of 9.9%, which was 27.7% smaller than that of the intact loess.

The above wetting induced volume change behavior of intact and compacted loess can be qualitatively interpreted using the loading collapse (LC) concept. Figure 6 shows the soil states of each sample before wetting with reference to LC curves. The initial LC curve was determined through the three yield points at suctions zero kPa, 50 kPa and 100 kPa (see in Figure 3a). For the intact loess at isotropic stresses of zero and 50 kPa, the wetting paths were mainly located within the elastic region

and hence elastic swellings were induced. For the intact loess at an isotropic stress of 200 kPa, the wetting path started from the elastic region and then touched the initial LC curve. Thus, it can be inferred that the intact loess first showed elastic swelling at the initial wetting stage (i.e. from 200 kPa to 100 kPa), followed by plastic collapse with further wetting from 100 kPa to zero kPa (see in Figure 5). Similar to the intact loess, the initial LC curve of the compacted loess was also determined through the three yield points at suctions zero kPa, 50 kPa and 100 kPa (see in Figure 4a). It was clear that the initial LC curve of the compacted loess displayed a smaller inclination than that of the intact loess, indicating a smaller collapse potential (Alonso et al., 1990). The wetting path of the compacted loess at an isotropic stress of zero kPa was also located within the initial LC curve and hence elastic swelling was observed (see in Figure 5). More importantly, for the compacted loess at an isotropic stress of 50 kPa, as the wetting path touched the initial LC curve, plastic collapse was induced during the wetting. The evolution of the LC curves can qualitatively explain the different wetting induced volume change behavior of the intact and compacted loess at an isotropic stress of 50 kPa. Additionally, at an isotropic stress of 200 kPa, the wetting path of intact and compacted loess touched the LC curve, thereby inducing plastic collapse. This was also consistent with the volume change behavior observed in Figure 5.

6. Interpretation of the collapse behavior of intact and compacted loess through microstructure analysis

6.1. SEM observations

Figure 7a shows the SEM image of intact loess at the initial state (see point A0 in Figure 2) with 200x magnification. As shown in the image, the aggregates formed by both silt and clay particles or solely by clay particles were widely observed, and the inter-aggregate and intra-aggregate pores could be identified. Similar dual pore structures were observed by Muñoz-Castelblanco et al. (2011), Jiang et al. (2012) and Ng et al. (2019) for the intact loess from northern France and northwest China. Moreover, extra-large pores with diameters of several hundred micrometres were observed in the intact loess. Due to the unstable structure, it was expected that those extra-large pores would be collapsed first during isotropic compression and wetting. To get a clear view of the particle arrangement, an SEM image of intact loess has been shown under 400x magnification in Figure 7b. Sub-angular silt grains with diameters of a few tens of micrometres dominated in the SEM micrographs. More importantly, based on the SEM image shown in Figure 7b, it is clear that clay and silt particles form aggregations (about 60 μm in diameter), with some small-size particles (<50 μm in diameter) accumulated at the inter-aggregate contacts. According to previous studies (Muñoz-Castelblanco et al., 2012; Ng et al., 2019), these small-size particles are able to enlarge the area of inter-aggregate contacts and hence stabilize soil skeleton. On the other hand, direct observation of calcite cementation through SEM image was difficult due to small dimension or special morphology, such as coatings or bridging. The presence of calcite cementation was confirmed through XRD measurements (see Figure 1). This calcite cementation and

the clay connections in the intact loess could result in a resistant soil structure, and hence, larger yield stresses than that of the compacted loess (see in Figures 3 and 4).

Figure 8a shows an SEM micrograph of the compacted loess in its initial state (see point A0 in Figure 2) under 200x magnification. The overall image is quite similar to that of the intact sample. Both inter- and intra-aggregate pores could be identified. The dual pore structure of the compacted loess was because the sample was compacted on the dry side of optimum water content (Delage et al., 1996; Ng et al., 2019). More importantly, the extra-large pores which were widely distributed in the intact loess could not be observed in the compacted loess. It was expected that the compression and wetting induced collapse of compacted loess was primarily due to the breakdown of inter-aggregate pores. The SEM image of compacted loess under 400x magnification was taken (Figure 8b) to further identify the particle arrangement. Similar to the image of intact loess, silt-size aggregates were also widely distributed in the micrograph. Furthermore, the image was quite different from that of the intact loess in terms of clay particle distribution. The silt particles preferred direct contacts without clay connections and calcite cementation. This is because the grinding and sieving during sample preparation dislodged the clay particles and calcite cementation that were accumulated near the grain contacts. In addition, the clay particles in the compacted loess seemed to mainly form silt-size aggregates or adhere on the surface of the silt grains. As the clay connections and calcite cementation were absent in the compacted loess, the soil skeleton of the compacted loess was expected to be weaker than that of intact loess.

6.2. MIP measurements

Figure 9 shows the pore size distributions of the intact loess in the initial state (point A0 in Figure 2) and after isotropic compression at suctions zero (point D1 in Figure 2a) and 50 kPa (point C1 in Figure 2a). In the initial state, the intact loess exhibited a bimodal pore size distribution defining a population of large (i.e. 8.2 μm) and small (i.e. 0·03 μm) pores. The bimodal pore size distribution of the intact loess was consistent with the SEM observations, which showed both inter and intra-aggregate pores. It should be noted that the extra-large pores present in the SEM micrograph (Figure 8a) were not observed in the MIP measurement. This was because of limited minimal pressure within the MIP apparatus which cannot accurately detect pores with diameters larger than 400 μm. For the intact loess after compression at suction zero kPa, the population of inter-aggregate pores (i.e., 8.2 μm) shifted toward smaller pore size (i.e., 3.1 μm). The compression occurred both for the extra-large and inter-aggregate pores. In addition, the intra-aggregate pores were almost not influenced by the isotropic compression. This result was similar to the previous experimental studies which showed that compression induced volume change of loess only occurred in the inter-aggregate pores but had no effects on the intra-aggregate pores (Jiang et al., 2012). For the intact loess after isotropic compression at a suction of 50 kPa, the pore size distribution became almost similar to that of the intact loess in its initial state, although the void ratio decreased by 12.6% (see Figure 3a). This was probably because the compression of soil was caused by the breakdown of the extra-large pores to relatively small sized pores which still

could not be identified by the MIP measurements. The constant pore size distributions of intact loess can explain the constant water content changes during isotropic compression (Figure 3b).

Figure 10 shows the pore size distributions of compacted loess in its initial state (point A0 in Figure 2a) and after isotropic compression at suctions of zero kPa (point D1 in Figure 2a) and 50 kPa (point C1 in Figure 2a). In the initial state, the compacted loess showed a bimodal pore size distribution, which was similar to that of the intact loess. The average intrusion diameters of inter- and intra-aggregate pores were 9.0 μm and 0.03 μm, respectively. After compression from zero kPa to 300 kPa at a suction of zero kPa, the population of the inter-aggregate pores shifted toward smaller pore size (i.e., 2.6 μm), but with a constant distribution of intra-aggregate pores. Thus, it can be inferred that the compression induced collapse influenced only the inter-aggregate pores in both the intact and compacted loess. For the soil samples compressed from zero to 300 kPa at a suction of 50 kPa, the population of the inter-aggregate pores shifted from an average intrusion diameter of 9.0 μm to 6.1 μm. According to Young-Laplace equation ($s=2T_s/r$, s is suction; T_s and r are surface tension coefficient of ice-water interface and pore radius, respectively, T_s = 72.75 mN/m at 20 ^oC) (Mu et al., 2018), a suction of 50 kPa corresponded to an intrusion pore diameter of 5.7 μm. It meant that the pores with diameters smaller than 5.7 μm would be filled in water with an applied suction of 50 kPa. From the measured pore size distributions, the volume of the pores smaller than 5.7 μm increased significantly during isotropic compression at a suction of 50 kPa.

Therefore, water flowed into these pores during compression whose consequence was a significant increase in the gravimetric water content (see in Figure 4b).

7. Summary and conclusions

It is well recognized that the behaviour of intact and compacted specimens are different, but there is no experimental study of the volume change behavior of intact and compacted loess specimens at unsaturated condition. This study provides comprehensive data to compare the volume change behavior between intact and compacted loess based on suction- and stress-controlled compression and wetting tests. In particular, a new finding of this study is that under isotropic compression at suctions of 50 and 100 kPa, the water content of intact and compacted specimens remain almost constant and increases by 4.4-7.5%, respectively. This difference is most likely related to the different pore size distributions of these two specimens. For the compacted specimen, soil pores become smaller under compression and hence tends to adsorb more water. On the contrary, the intact specimen has some large-size pores with a diameter larger than 400 μm, as evidenced by MIP tests. These large-size pores are expected to be dry at suctions of 50 and 100 kPa, based on the Young-Laplace equation. Consequently, the collapse of these large-size pores does not change the water content of intact loess. Furthermore, this new finding is helpful for improving the understanding of hydro-mechanical coupled behaviour of unsaturated loess.

The yield stresses of intact loess were 42.3%, 43.6% and 52.5% larger than that of the compacted loess at suctions zero kPa, 50 kPa and 100 kPa, respectively. The

stiffer compression behavior of intact loess was mainly because of the resistant soil structure contributed by clay particles and calcite cementation.

Acknowledgement

The authors would like to acknowledge the financial support provided by the Research Grants Council of the Hong Kong Special Administrative Region (HKSAR) (grant no. 16204817, 16207417 and AoE/E-603/18), the National Science Foundation of China (grant no. 51909205 and 51778166), the China Postdoctoral Science Foundation (grant no. 2018M631166 and 2019T120914), and the Fundamental Research Funds for the Central Universities of China (grant no. xjj2018250).

References：

Alonso EE, Gens A, Josa A. A constitutive model for partially saturated soils. Géotechnique 1990; 40(3): 405-430.

ASTM D2478. Standard practice for classification of soils for engineering purposes (Unified Soil Classification System) American Society for Testing and Materials, West Conshohocken, Pa; 2006.

Behnood A. Soil and clay stabilization with calcium-and non-calcium-based additives: A state-of-the-art review of challenges, approaches and techniques. Transp. Geotech. 2018; 17: 14-32.

Delage P, Audiguier M, Cui YJ, Howat MD. Microstructure of a compacted silt. Can. Geotech. J. 1996; 33(1): 150-158.

Garakani AA, Haeri SM, Khosravi A, Habibagahi G. Hydro-mechanical behavior of

undisturbed collapsible loessial soils under different stress state conditions. Eng. Geol. 2015; 195: 28-41.

Garakani AA, Haeri SM, Cherati DY, Givi FA, Tadi MK, Hashemi AH, Chiti N, Qahremani F. Effect of road salts on the hydro-mechanical behavior of unsaturated collapsible soils. Transp. Geotech. 2018; 17: 77-90.

Haeri SM, Khosravi A, Garakani AA, Ghazizadeh S. Effect of soil structure and disturbance on hydromechanical behavior of collapsible loessial soils. Int. J. Geomech. 2016; 17(1): 04016021.

Ji J, Zhang C, Gao Y, Kodikara J. Effect of 2D spatial variability on slope reliability: a simplified FORM analysis. Geosci. Front. 2018; 9 (6): 1631-1638.

Ji J, Zhang C, Gao Y, Kodikara J. Reliability-based design for geotechnical engineering: An inverse FORM approach for practice. Comput. Geotech. 2019; 111: 22-29.

Jiang MJ, Hu HJ, Liu F. Summary of collapsible behaviour of artificially structured loess in oedometer and triaxial wetting tests. Can. Geotech. J. 2012; 49(10): 1147-1157.

Jiang M, Zhang F, Hu H. DEM Modeling Mechanical Behavior of Unsaturated Structural Loess under Constant Stress Increment Ratio Compression Tests. Int. J. Geomech. 2016; 17(4): 04016108.

Liu Z, Liu FY, Ma FL, Wang M, Bai XH, Zheng YL, Yin H, Zhang GP. Collapsibility, composition, and microstructure of loess in China. Can. Geotech. J. 2015; 53(4): 673-686.

Ma F, Yang J, Bai X. Water sensitivity and microstructure of compacted loess. . Transp. Geotech. 2017; 11: 41-56.

Muñoz-Castelblanco JA, Delage P, Pereira JM, Cui YJ. Some aspects of the compression and collapse behaviour of an unsaturated natural loess. Géotech. Lett. 2011; 1(2): 17-22.

Muñoz-Castelblanco JA, Pereira JM, Delage P, Cui, YJ. The water retention properties of a natural unsaturated loess from northern France. Géotechnique. 2012; 62(2): 95-106.

Mu QY, Ng CWW, Zhou C, Zhou GGD. A new model for capturing void ratio-dependent unfrozen water characteristics curves. Comput. Geotech. 2018; 101: 95-99.

Mu QY, Dong H, Liao HJ, Dang YJ, Zhou C. Water retention curves of intact, compacted and reconstituted loess under cyclic wetting-drying. Géotechnique Lett. 2020; 10(1): 1-6.

Ng CWW, Cheng Q, Zhou C. Thermal effects on yielding and wetting-induced collapse of recompacted and intact loess. Can. Geotech. J. 2018; 55(8): 1095-1103.

Ng CWW, Mu, QY, Zhou C. Effects of soil structure on the shear behaviour of an unsaturated loess at different suctions and temperatures. Can. Geotech. J. 2016a; 54(2), 270-279.

Ng CWW, Sadeghi H, Hossen SKB, Chiu CF, Alonso EE, Baghbanrezvan S. Water retention and volumetric characteristics of intact and re-compacted loess. Can.

Geotech. J. 2016b; 53(8): 1258–1269.

Ng CWW, Mu QY, Zhou C. Effects of specimen preparation method on volume changes of clay under cyclic thermal loads. Géotechnique. 2019; 69(2): 146-150.

Sivakumar V. A critical state framework for unsaturated soils. Ph.D. thesis, University of Sheffield, UK. 1993.

Wang XL, Zhu YP, Huang XF. Field tests on deformation property of self-weight collapsible loess with large thickness. Int. J. Geomech. 2014; 14(3): 04014001.

Wheeler SJ, Sharma RS, Buisson MSR. Coupling of hydraulic hysteresis and stress–strain behaviour in unsaturated soils. Géotechnique. 2003; 53(1):41-54.

Zhan TLT, Yang YB, Chen R, Ng CWW, Chen YM. Influence of clod size and water content on gas permeability of a compacted loess. Can. Geotech. J. 2014; 51(12): 1468-1474.

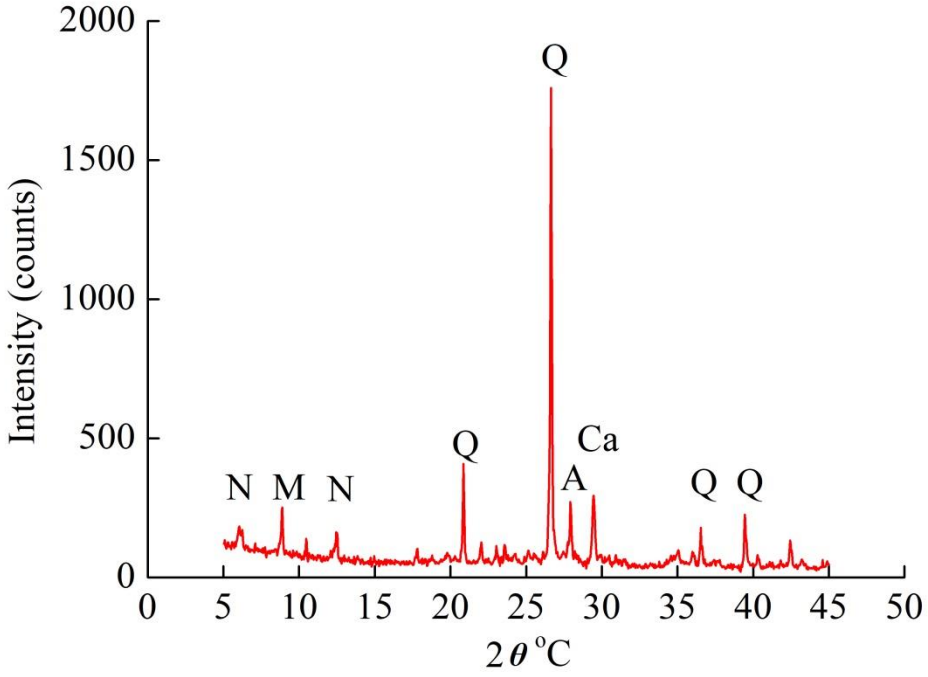

Figure 1 X-ray diffraction pattern of the tested loess

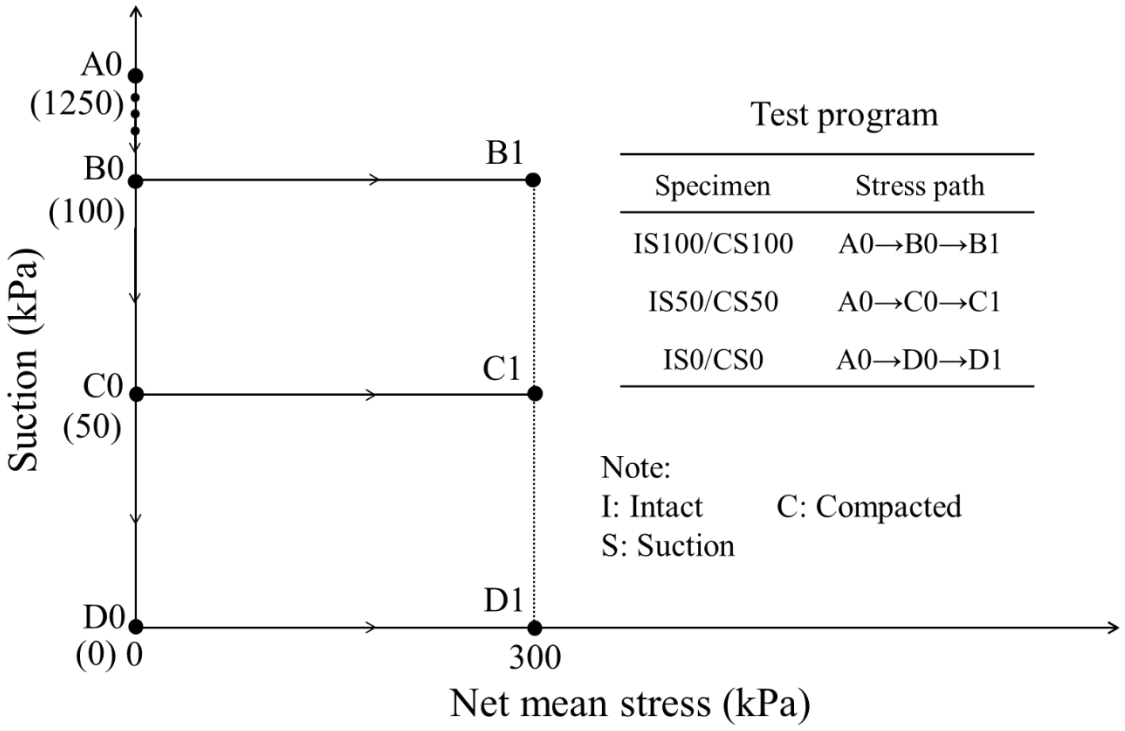

(a)

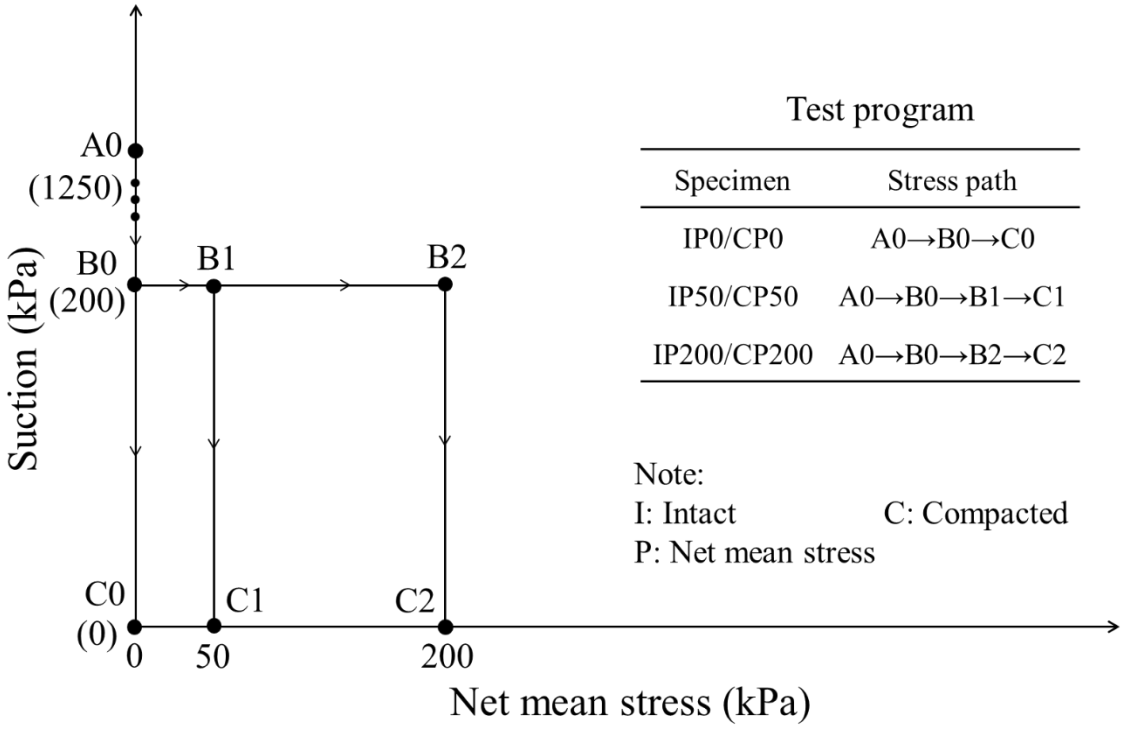

(b)

Figure 2 Stress path and test program: (a) isotropic compression tests; (b) wetting induced collapse tests

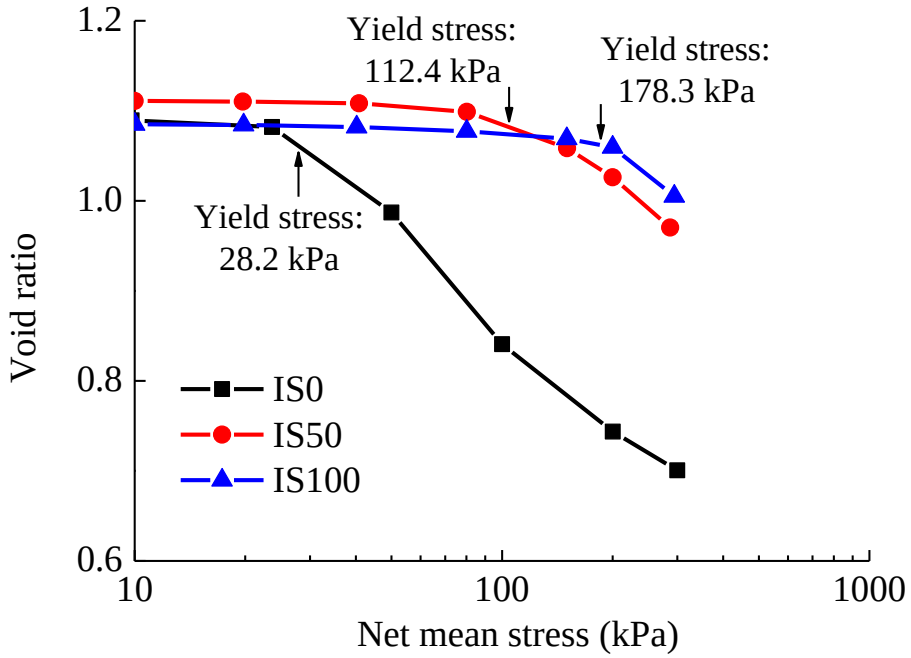

(a)

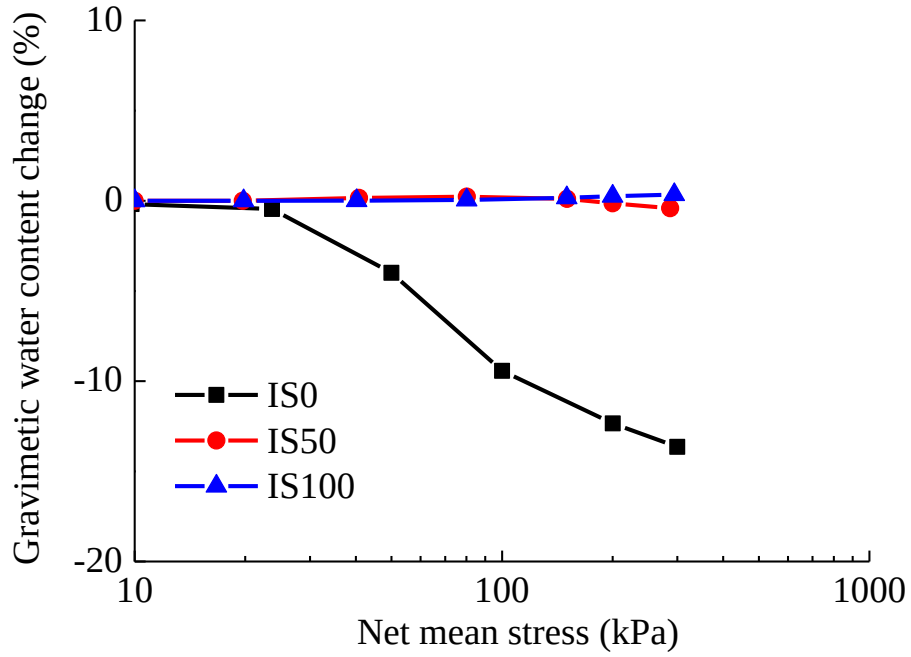

(b)

Figure 3 Compression behavior of intact loess at constant suctions: (a) deformation; (b) gravimetric water content changes

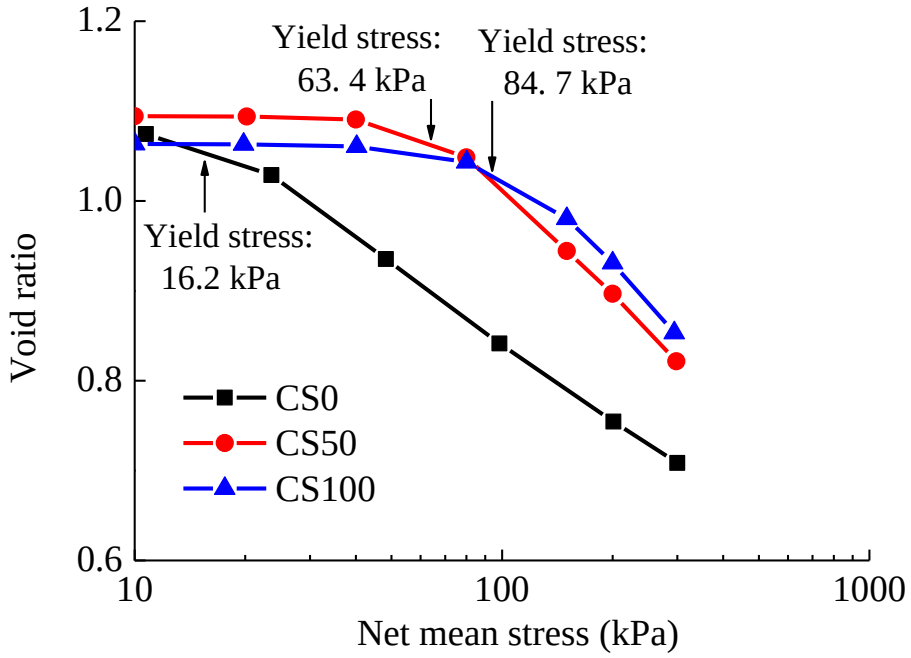

(a)

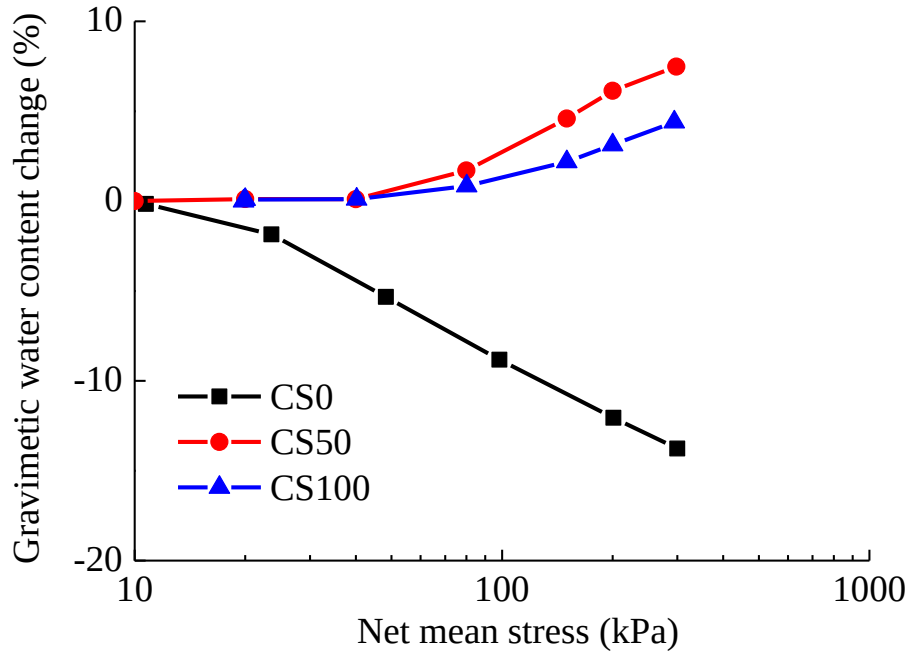

Figure 4 Compression behavior of compacted loess at constant suctions: (a) deformation; (b) gravimetric water content changes

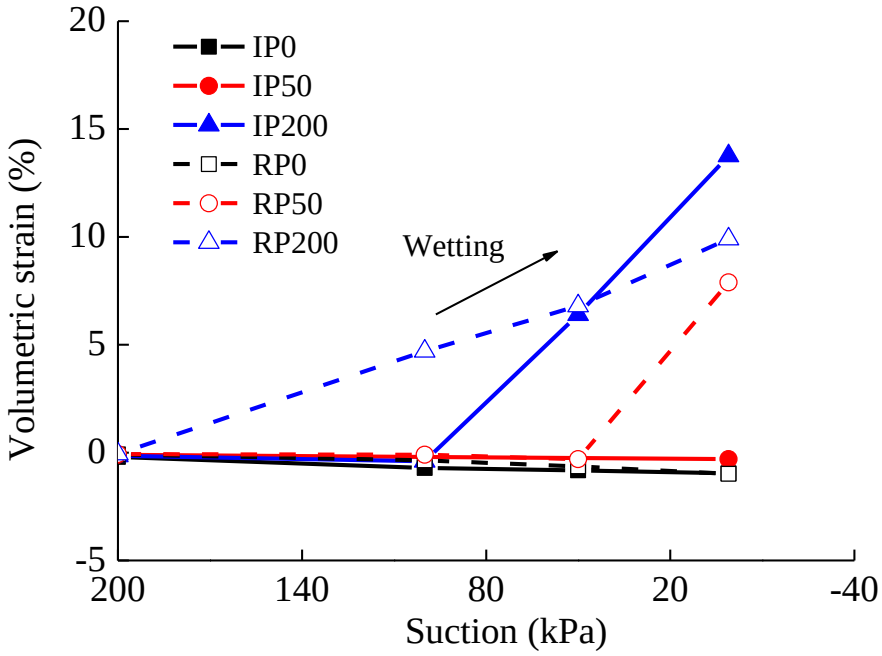

Figure 5 Wetting induced volume changes of intact and compacted loess at constant stress conditions

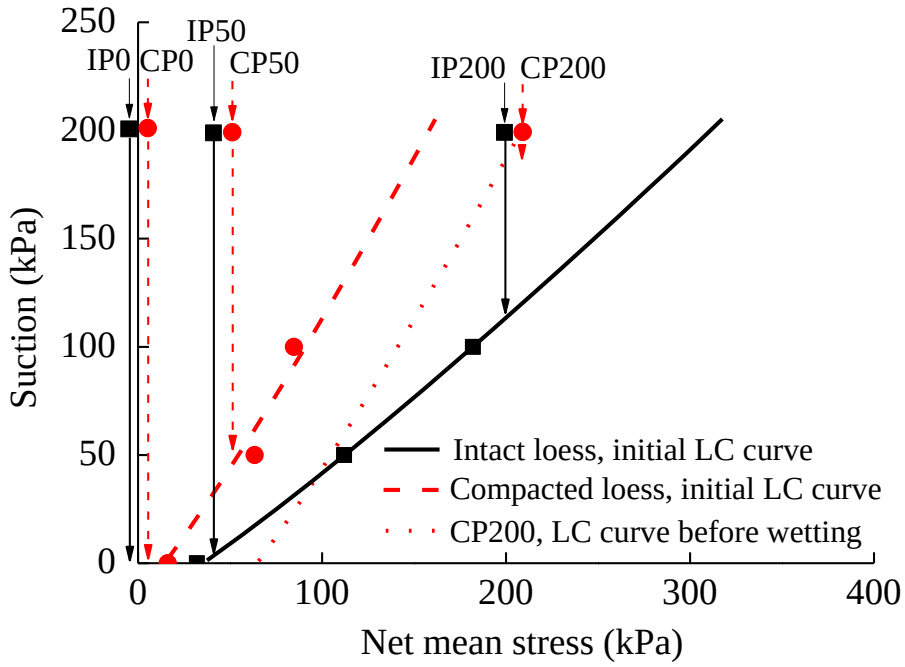

Figure 6 Illustration of volume change of intact and compacted loess within the framework of LC concept

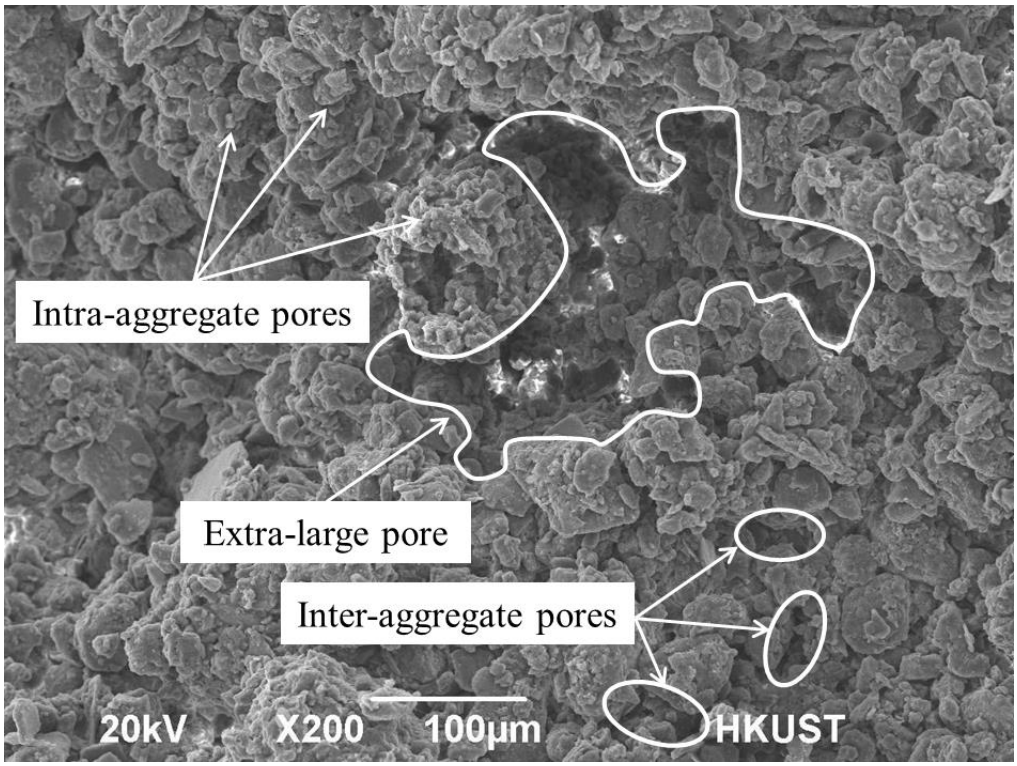

(a)

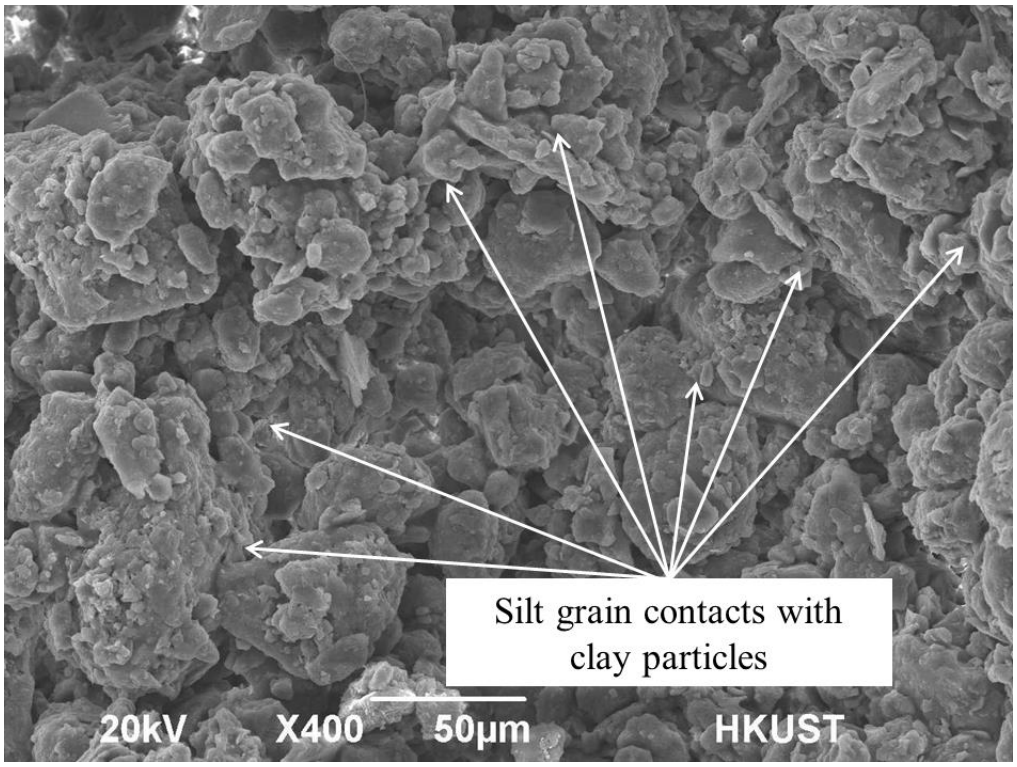

(b)

Figure 7 SEM observations of intact loess at the initial state: (a) magnification ×200; (b) magnification ×400

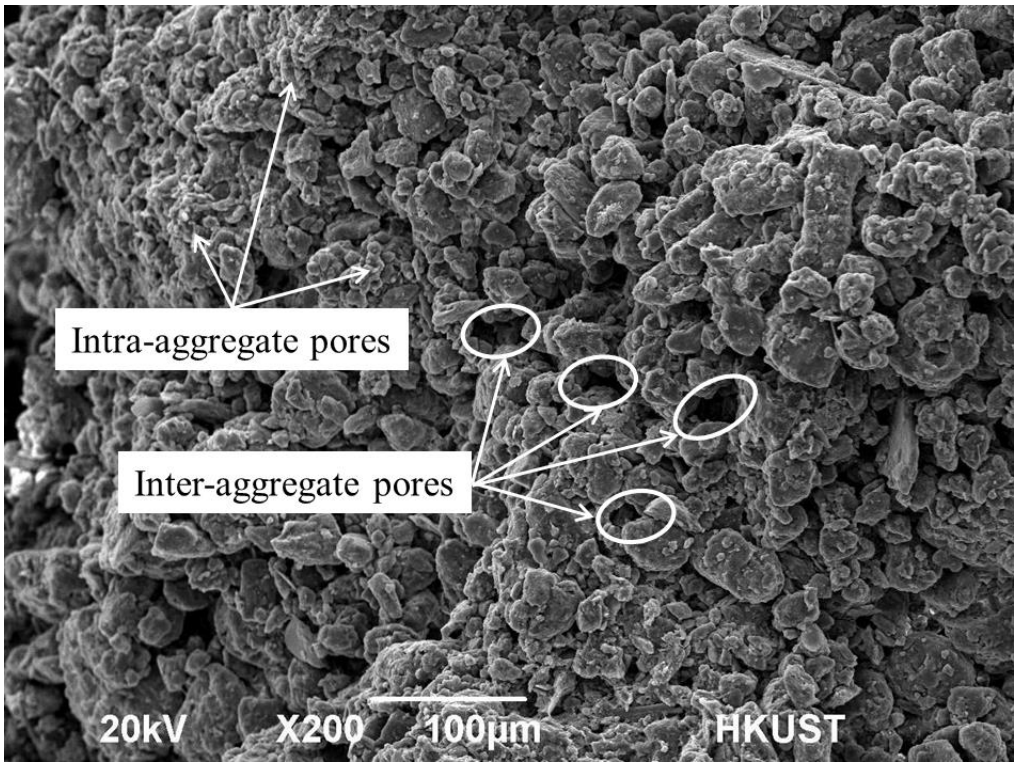

(a)

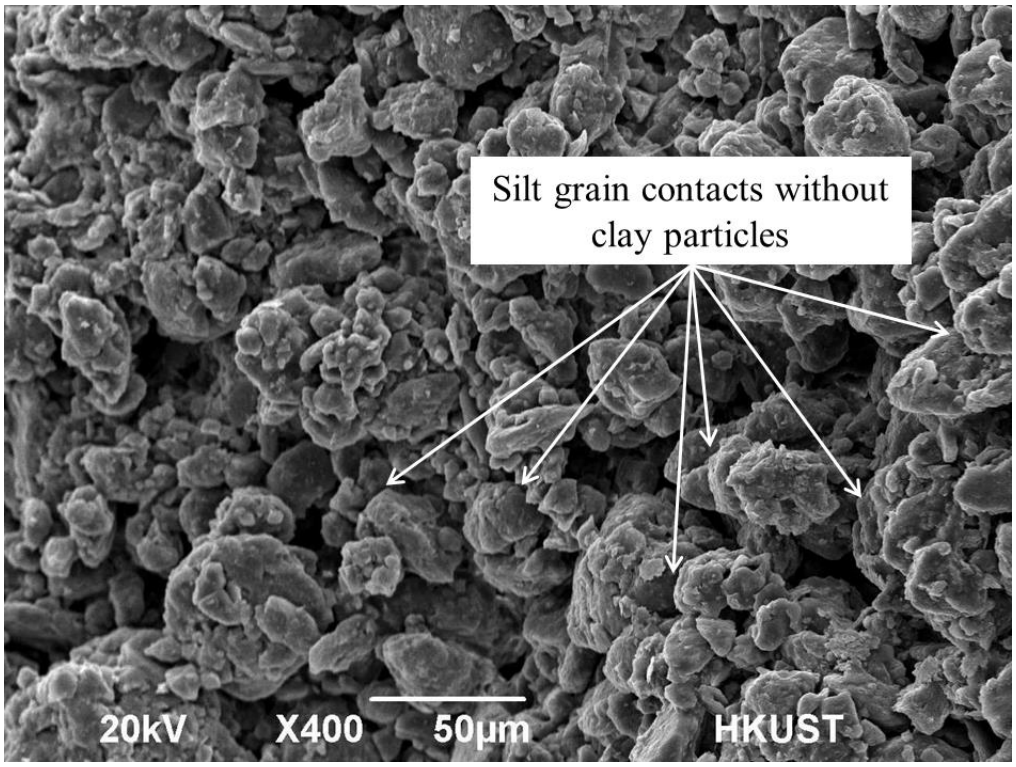

(b)

Figure 8 SEM observations of compacted loess at the initial state: (a) magnification ×200; (b) magnification ×400

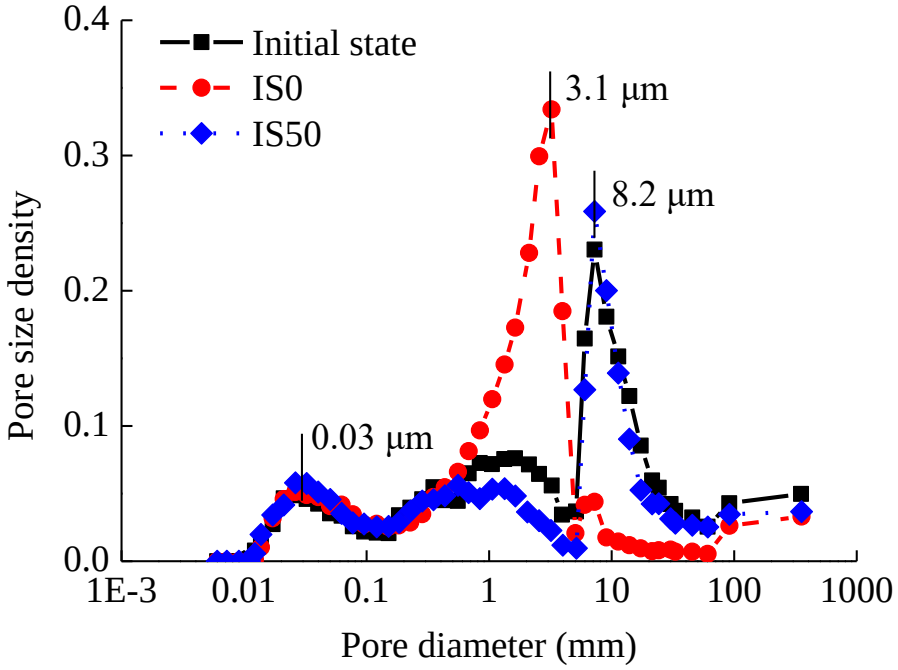

Figure 9 Pore size distributions of intact loess at the initial state (see point A0 in Figure 2a) and after isotropic compression at suction of 50 kPa (see point C1 in Figure 2a) and zero kPa (see point D1 in Figure 2a)

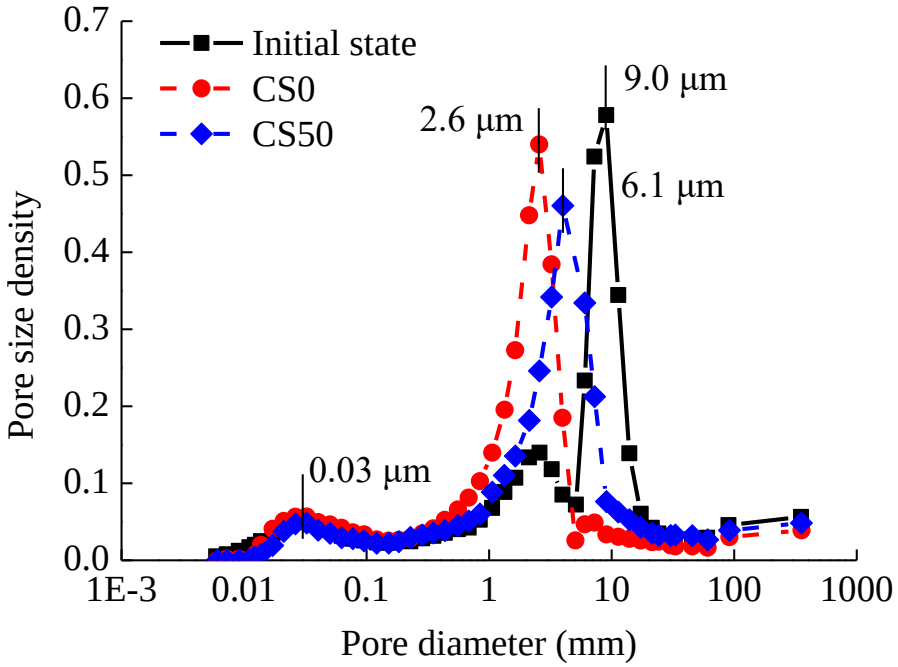

Figure 10 Pore size distributions of compacted loess at the initial state (see point A0 in Figure 2a) and after isotropic compression at suction of 50 kPa (see point C1 in Figure 2a) and zero kPa (see point D1 in Figure 2a)